*inventions*

MDPI

*Article*

# Effect of Different Contents of 63s Bioglass on the Performance of Bioglass-PCL Composite Bone Scaffolds

**Chen Zhang [1,†], Shihao Chen [2,†], Muniyandi Vigneshwaran [3,4], Yi Qi [1,2], Yulai Zhou [2], Gaosheng Fu [1], Zhiyu Li [1,*] and Jianlei Wang [3,*]**

1 School of Materials and Chemistry Engineering, Minjiang University, Xiyuangong Road No. 200, Fuzhou 350108, China; zhangchen@mju.edu.cn (C.Z.); qiyi23@mails.jlu.edu.cn (Y.Q.); fugaosheng@fzu.edu.cn (G.F.)
2 School of Pharmaceutical Sciences, Jilin University, Changchun 130021, China; shchen21@mails.jlu.edu.cn (S.C.); zhouyl@jlu.edu.cn (Y.Z.)
3 CAS Key Laboratory of Design and Assembly of Functional Nanostructures, Fujian Key Laboratory of Nanomaterials, Fujian Institute of Research on the Structure of Matter, Chinese Academy of Sciences, Fuzhou 350002, China; m.vignesh@fjirsm.ac.cn
4 University of Chinese Academy of Sciences, Beijing 100049, China
* Correspondence: lzhiyu@mju.edu.cn (Z.L.); jlwang@fjirsm.ac.cn (J.W.)
† These authors contributed equally to this work.

**Abstract:** Bioactive glasses (BG), notably 63s BG, possess distinct properties such as biodegradability, biocompatibility, and the ability to boost cellular interactions. Our research concentrated on formulating polycaprolactone (PCL) porous scaffolds enriched with 63s BG to gauge their combined mechanical and biological potentials. Using twin-screw extrusion, we created composites containing 5%, 10%, and 20% 63s BG. These were transformed into cylindrical scaffolds using 3D printing. Our assessments involved melt flow, SEM, XRD, water contact angle metrics, DSC, and extracorporeal degradation. After co-culturing with MC3T3-E1 cells, an uptick in alkaline phosphatase activity was noted. Preliminary findings demonstrated that as 63s BG content increased, the properties of the composites improved. Yet, they fell short of replicating the mechanical nuances of cortical bone, rendering them inapt for load-bearing orthopedic applications but suitable for mending minor bone defects or cartilage. In summary, while 63s BG brings about significant advancements in scaffold attributes, attaining the mechanical traits ideal for certain medical purposes remains elusive. This investigation offers foundational insights for the evolution of optimized bone tissue engineering materials.

**Keywords:** 3D printing; bioactive glasses; bone regeneration; 63s



**Citation:** Zhang, C.; Chen, S.; Vigneshwaran, M.; Qi, Y.; Zhou, Y.; Fu, G.; Li, Z.; Wang, J. Effect of Different Contents of 63s Bioglass on the Performance of Bioglass-PCL Composite Bone Scaffolds. *Inventions* **2023**, *8*, 138. https://doi.org/10.3390/inventions8060138

Academic Editor: Joshua M. Pearce

Received: 31 August 2023
Revised: 15 October 2023
Accepted: 16 October 2023
Published: 30 October 2023



## 1. Introduction

Bone defects result from metabolic or degenerative diseases, bone tumor resection, infection, trauma, and other congenital or acquired factors. While human bone tissue has some regenerative ability, its capacity is limited and can be affected by various pathological factors, making bone defect treatment a challenging problem in clinical work [1,2]. Autologous bone transplantation is currently the preferred material for the clinical treatment of bone defects [3,4]. However, limited autologous bone quantity and prolonged operation time are major shortcomings [5]. Therefore, with the integration and development of medicine and materials science, artificial material orthopedic implants have gained popularity as a replacement for autologous bone transplantation [6,7].

Three-dimensional (3D) printing is a revolutionary technology that enables the fabrication of structures directly from digital models. Since its inception in the 1980s, the technology has evolved tremendously and has come into service in manufacturing, healthcare, aerospace, and more [8,9]. Three-dimensional printing has revolutionized production

processes by allowing rapid prototyping, reducing waste, and enabling the creation of complicated designs [10,11].

The allure of 3D printing is its capacity for customization and rapid prototyping. Engineers, medical workers, artists, and consumers can now design and print complex structures that were previously impossible or too expensive to produce [12,13]. For example, in the medical field, 3D printing is used to create patient-specific implants and prosthetics, thereby increasing the likelihood of successful surgeries and fittings [14].

Another game-changing advantage is that of decentralized manufacturing. With the widespread availability of 3D printers and open-source design software, anyone can become a creator or manufacturer from the comfort of their own home or local maker space. This democratizes the production process and significantly reduces the lead time and logistics costs involved in getting a product from the manufacturer to the consumer [15].

In tissue regeneration, 3D printing has brought remarkable innovation, including bio-printed tissues and personalized pharmaceutical delivery [14,16,17]. Despite these advances, 3D printing also presents challenges, such as issues related to material properties, printing speed, and the environmental impact of the materials used [18,19].

Methods for making scaffolds range from conventional techniques such as solvent casting, particulate leaching, gas foaming, and freeze-drying to advanced techniques such as electrospinning and additive manufacturing or 3D printing [20–22]. The materials used to build these scaffolds are often biocompatible and biodegradable, including natural polymers, synthetic polymers, ceramics, and composites [23–25].

The application of 3D printing has been an innovation in the field of tissue engineering and regeneration [16]. Three-dimensional bioprinting offers the capability to fabricate bioengineered scaffolds that closely resemble the natural construction of tissues and organs [26,27]. These 3D-printed scaffolds are pivotal in diverse applications, such as studying disease pathogenesis, drug testing, tissue replacement, and organ transplantation [28–30].

Polycaprolactone (PCL) is a semi-crystalline, biodegradable polymer that has attracted interest in the field of biomaterials due to its excellent mechanical properties, biocompatibility, and slow degradation rate [31,32]. Synthesis of polycaprolactone by ring-opening polymerization (ROP) usually uses caprolactone (ε-caprolactone) as a monomer and tin (II) 2-ethylhexylate as a catalyst. In a reactor with a magnetic stirrer and temperature controller, the catalyst and caprolactone monomer are dried to remove water, and then the catalyst, caprolactone, and an optional ring-opener (e.g., propylene glycol) are mixed under anhydrous and oxygen-free conditions. Within a set temperature range (usually 60–150 °C) the reaction is carried out to form PCL. After the reaction is complete, purification and drying steps are usually required to obtain a high-purity PCL. Its unique properties make it suitable for a wide range of applications, including tissue engineering, drug delivery, and medical implant devices [33–35]. In 2014, Temple et al. achieved the successful development of a specialized 3D-printed polycaprolactone (PCL) scaffold that accurately constructs complex anatomical shapes and regulates porosity, demonstrating great potential in treating large craniomaxillofacial bone defects. Furthermore, studies have highlighted these scaffolds' outstanding biological properties by promoting the angiogenesis and osteogenesis of human adipose stem cells, thus providing effective support for bone tissue engineering [36]. PCL can be enhanced by mixing with other polymers to meet specific application needs [37–39]. Despite its numerous advantages, there are still some challenges that must be overcome, such as its hydrophobic nature and poor mechanical properties [40,41].

Bioactive glass was originally developed by Hench in 1969 to promote tissue regeneration, angiogenesis, and antimicrobial properties [42–45]. They are mostly composed of $Na_2O$, CaO, $P_2O_5$, and $SiO_2$. These biomaterials have received considerable attention over the past few decades due to their properties in bone tissue engineering and medical applications [46]. This capacity for bonding tissues, mainly bone, derives from a series of surface reactions that lead to the formation of a layer of carbonated hydroxyapatite, which is chemically and structurally similar to bone [47]. They have found applications

in orthopedics, dentistry, and even drug delivery [48–51]. By changing the content of the main components, such as sodium dioxide, calcium oxide, and phosphorus, bioactive glasses with different properties can be developed [47,52–54]. In addition, many in vitro and in vivo, studies on bioglass have shown that this material can be used to produce scaffolds for tissue engineering. Therefore, they can be considered a promising scaffold material. The scaffold is a 3D structure, and because of its porous structure, it allows cells to attach to it and grow, which is conducive to blood vessel formation. On the other hand, biological scaffolds should have sufficient mechanical strength to bear weight [55].

Bioactive glass has many advantages in the fields of medicine and biomaterials, but there are also some limitations or disadvantages [56]. Traditional bioglass typically does not have very high mechanical strength, which limits its use in situations where it is subjected to large forces, such as weight-bearing bones. Furthermore, the rate of degradation of bioglass needs to be carefully controlled to match the rate of tissue regeneration. Too fast or too slow degradation may harm the ultimate therapeutic effect. Due to the above limitations, bioglass is mainly used in non-weight-bearing areas, such as dental implants and some soft tissue engineering [42,43,57–59].

The effects of 63s content on the properties of composite scaffolds were studied. We concluded that although the performance of the composite material increased with the increase of BG content, its strength was still insufficient for the implantation of load-bearing bone, but it could repair small-volume bone defects and non-load-bearing bone.

## 2. Materials and Methods

### *2.1. Fabrication of 3D-Printed PCL, PCL/63s Scaffolds*

The fabrication procedure of the 3D-printed PCL and PCL/63s scaffolds begins by blending PCL with varying mass fractions (5%, 10% and 20%) of BG. (Kunshan Chinese Technology New Materials Co., Ltd., Kunshan, China), Ca/P = 6.546, particle size range 0–80 μm. These resulting composites constitute three parallel experimental groups, labeled PCL@[1]5, PCL@63sBG10, and PCL@63sBG20, each corresponding to a distinct 63s BG mass fraction. Meanwhile, pure PCL is designated as the control group. Before blending, the 200 mesh PCL (Capa 6500; SOLVAY, Alorton, IL, USA) particles were dried in an air blast drying (XMTD-8222, Shanghai Jinghong Experiment Instrument Co., Ltd., Shanghai, China) oven for 8 h, and the drying temperature was set at 40 °C.

Step 1. Different BG/PCL composites were prepared by accurately weighing and mixing various weight percentages of 63s BG (Kunshan Huaqiao New Materials Co., Ltd., Suzhou, China) into PCL.

Step 2. The composites were mixed on a double-roll open molding machine (LN-LT-4, Guangdong Lina Industrial Co., Ltd., Dongguan, China) at a temperature of 45 °C. Rectangular strips of approximately 100 mm × 40 mm × 2 mm were cut and then pelletized using a granulator (JD1A-90, Shanghai Delixi Switch Co., Ltd., Shanghai, China).

Step 3. The composite material particles were passed through a twin-screw extruder (PloyLAb Os, Thermo Fisher Scientific, Bremen, Germany) to prepare strands for 3D printing composite scaffolds. Processing temperature according to the process section in turn: 60 °C, 75 °C, 90°C, 75 °C, 60 °C. Screw speed: 150 r/min.

Step 4. Due to the physical property differences between 63s BG and PCL, the prepared strands initially had non-uniform cross-section diameters and burls, making them unsuitable for the 3D printing scaffolds. To address this issue, the strands need to be converted into composite material particles again using a granulator. The steps of Step 3 should be repeated several times (generally 3–4 times) until the diameter of the line is approximately 1.75 mm, ensuring that there are no burrs or protrusions on the surface. A stand model designed with Solidworks 2022 should be printed using a 3D printer (Snapermaker 2.0 A350, Shenzhen Snapmaker Technologies Co., Ltd., Shenzhen, China).

The composite scaffold printing process involves first digitally modeling the scaffold and then using FDM technology to print four groups of material scaffolds using composite and pure PCL material strands prepared as raw material.

First, Solidworks 2022 was used to design a three-dimensional model of the composite bone scaffold and generate a digital model file for precise manufacturing using a numerical control system. The scaffold was cylindrical with a bottom diameter of 10 mm, a height of 3 mm, and a porosity of 50%. Then, the printing process parameters: printing speed 5 mm/s, printing height 0.28 mm, room temperature 20 °C, nozzle temperature 80 °C, hot bed temperature 45 °C. The process parameters in the printing process are controlled by Snapmaker Luban 4.7.2.

The entire procedure of scaffolds fabrication is depicted in Figure 1.

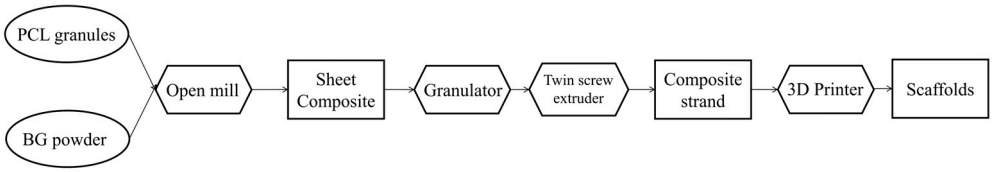


**Figure 1.** The process of making scaffolds.

### *2.2. Characterization of Scaffolds and 63s Powder*

Macro- and micromorphology of the composite scaffolds: a total of 12 scaffolds were obtained by randomly selecting three 3D-printed composite bone scaffolds from each of the three parallel experimental groups, PCL@63sBG5, PCL@63sBG10, PCL@63sBG20, and a control group, which exclusively comprised pure PCL. The diameter, and height of these scaffolds were individually measured by vernier calipers (Shanghai Tools Factory Co., Ltd., Shanghai, China), and the weight of them was measured by a precision balance (Kunshan Science Instruments Co., Ltd., Kunshan, China). The average values were calculated based on the collected data. To observe the microstructural characteristics of the composite scaffold images were captured using SEM (E-1045, HITACHI; Tokyo, Japan) at 65×. The 63s BG powder images were captured using SEM at 1000×, 5000×, 10,000×, and 20,000×. The composite images were collected by SEM at 1000×.

### *2.3. X-ray Diffraction (XRD) Analysis*

First, pure PCL composite materials containing 5%, 10%, and 20%63s BG were prepared into samples with a diameter of 20 mm and a thickness of 1 mm, and tested in the X-ray diffractometer (Rigaku MiniFlex 600; Rigaku, Tokyo, Japan) together with powdered 63sBG. The voltage was set to 40 kV, the current was set to 15 mA, the 2θ range was from 5° to 40°, the scanning speed was set to 4° per minute, and finally, the data were processed and analyzed using the XRD analysis software (MDI Jade 6), and the origin 2022 was used for mapping.

### *2.4. Melt Flow Rate*

After the BG and PCL are mixed by twin screws, the thread material is cut into pellets. The particle samples were divided into four groups: pure PCL, mixed material containing 5% BG, mixed material containing 10% BG, and mixed material containing 20% BG. To test the melting index of composite materials with different proportions, the composite material was heated to 125 °C and 2.16 kg of pressure was added in the melt flow rate tester (XNR-400A; Chengde Dajia Instrument Co., Ltd., Chengde, China) according to ASTM D1238.

### *2.5. Heating Rheological Test*

First, the granular sample is pressed into a plate vulcanizer with a thickness of 1 mm and a diameter of 2 cm. Then the samples were divided into four groups: pure PCL, mixed material containing 5% BG, mixed material containing 10% BG, and mixed material containing 20% BG. To analyze how the viscosity of the composite changes during the heating process, the material is heated from 75 °C to 120 °C, and its loss angle tangent and

energy storage modulus are measured by a polymer rotary rheometer system (DHR-2, TA Instruments; New Castle, DE, USA).

### *2.6. Differential Scanning Calorimetry*

The granular samples were also divided into four groups. At the same heating rate, the composites were heated above the melting point, and the melting points of the composites with different proportions were measured by differential scanning calorimetry (DSC 25, TA Instruments; New Castle, DE, USA). To eliminate the thermal history, secondary heating is performed.

### *2.7. Contact Angle*

The samples were also divided into four groups after hot pressing by the plate vulcanizer. The support was measured with a contact angle goniometer (JC2000D, Shanghai Zhongchen Digital Technology Equipment Co., Ltd., Shanghai, China). Three samples were selected from each group for analysis. The contact angle is measured by image processing.

### *2.8. Modulus of Elasticity*

One sample was selected from each of the four groups. The melted granular sample is poured into the mold to make cuboid samples and divided into four groups. The elastic modulus of the composite is measured by slowly compressing the material in a multipurpose tester (AG-X plus 100 KN; SHIMADZU) and recording the stress and strain.

### *2.9. In Vitro Degradation Rate*

To further observe the simulated in vivo degradation rate of composite scaffolds, scaffolds were chosen at random for experimental groups PCL@63sBG5, PCL@63sBG10, and PCL@63sBG20, and a control group ($n$ = 4). After recording their mass, each scaffold was disinfected with a 75% ethanol solution for roughly 30 min before air drying on a sterile, ultra-clean operating table. The scaffolds were then immersed in 30 mL of simulated body fluids (SBF, Beijing Leagene Biotechnology Co., Ltd., Beijing, China) and placed into 50 mL cell culture flasks with a culture area of 25 $cm^2$, incubated at 37 °C, and observed. One scaffold from each group was removed, degraded, and dried to a constant mass in an air-blast drying oven at 40 °C every 7 days. The change in dry weight and mass of each group was recorded throughout the 28-day experiment. The weight loss rate (Δ) was calculated using a specific formula.

$$\Delta\ (\%) = [(W_0 - W_t)/W_0] \times 100\% \quad (1)$$

In the formula, Δ is the weight loss rate, $W_0$ is the weight of each stent before degradation, and $W_t$ is the weight of the stent removed per week.

### *2.10. Alkaline Phosphatase Activity Detection*

To verify the effect of composite materials on the bone formation ability of cells, the experiment was divided into two groups: the control group with normal culture and the experimental group with the addition of 20% 63s BG round sheet composite sample. The samples with a diameter of 2 cm and a thickness of 1 mm were prepared and cultured with MC3T3-E1 cells with a concentration of $1 \times 10^5$ cells/mL in a six-well plate for 72 h at 37 °C and 5% $CO_2$, and then stained with an alkaline phosphatase detection kit (Beyontime, C3206, Nantong, China). The cells were washed twice with buffer solution and fixed with 4% paraformaldehyde fixative solution, stained and incubated for 20 min, and observed under a microscope.

## 3. Results and Discussion

### *3.1. Morphology Observations*

At room temperature, the 63s BG powder stored in a glass container appears as a white, uniform, and fine powder with no visible macroscopic crystals or defects, as seen in Figure 2a.

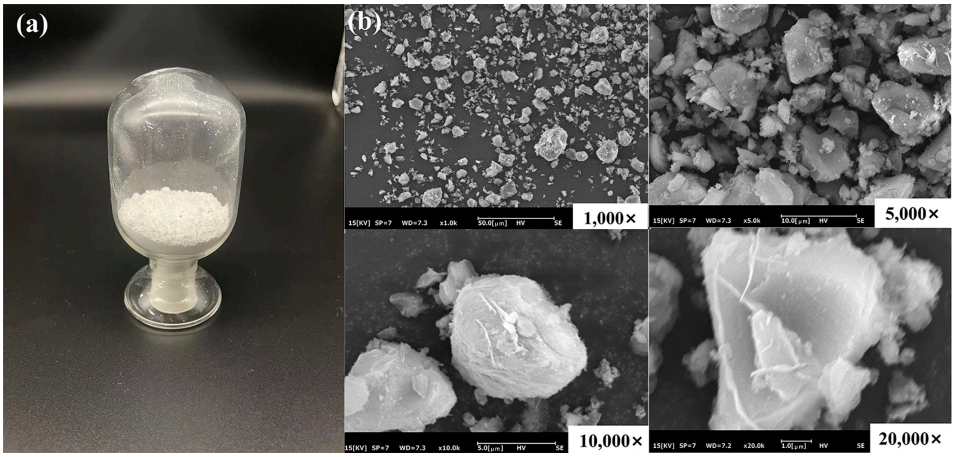


**Figure 2.** (**a**) Macro state of BG powder in a glass container. (**b**) Microstructure of BG powder under SEM.

Under the SEM, the microscopic morphology of 63s BG powder is shown in Figure 2b at magnifications of 1000×, 5000×, 10,000× and 20,000×. The particle size typically ranges from 0.1 to 5 μm and has an irregular spherical or lump-like shape with uniform particle distribution.

Both excessively high and low pore sizes are unfavorable for cell adhesion. In general, the porosity of artificial bone scaffolds is typically comparable to that of human trabecular bone, ranging from 30% to 90%. Within this range, the porosity is considered optimal [60–62]. To facilitate cell attachment, the scaffolds were set with a 50% porosity. Figure 3 displays that the BG/PCL composite bone scaffolds feature a cylindrical macroscopic morphology with a diameter measuring approximately 10 mm and a height of approximately 3 mm. An increase in the concentration of 63s BG heightened the color of the scaffold by altering it from white to slightly gray. Table 1 shows the weight, diameter, and height measurements of the composite scaffolds. The statistical method of single-factor analysis was employed to assess the weight, diameter, and height of the stent. The obtained *p*-values for weight, diameter, and height were 0.73, 0.90, and 0.72, respectively. All of these *p*-values exceeded the predetermined significance level of 0.05, indicating a lack of significant differences in these parameters among the different groups. Additionally, the standard deviation (σ) of each measurement item within the group was found to be less than 0.5, suggesting a low variance in weight, diameter, and height for the 3D-printed PCL-based bone scaffolds, and demonstrating excellent repeatability of the scaffold fabrication.

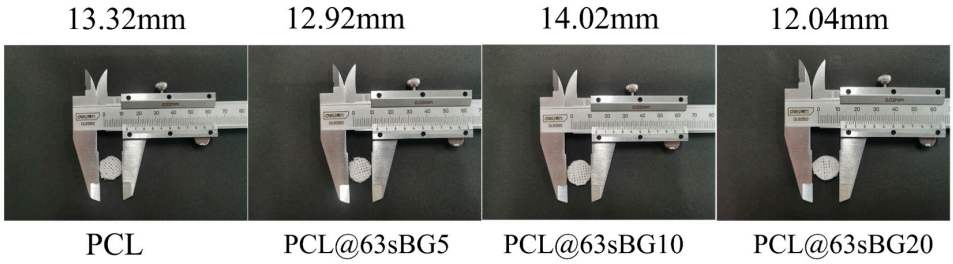


**Figure 3.** Macro topography of composite bone scaffolds.

**Table 1.** Measurement results of weight, diameter, and height of composite scaffolds.

| Group \ Scaffolds | | 1 | 2 | 3 | Average | σ |
|---|---|---|---|---|---|---|
| PCL | Weight (g) | 0.29 | 0.22 | 0.27 | 0.26 | 0.0294 |
| | Diameter (mm) | 13.32 | 13.40 | 13.24 | 13.32 | 0.0653 |
| | Height (mm) | 2.98 | 3.02 | 3.04 | 3.01 | 0.0249 |
| PCL@63sBG5 | Weight (g) | 0.36 | 0.35 | 0.33 | 0.35 | 0.0125 |
| | Diameter (mm) | 12.92 | 13.04 | 12.86 | 12.94 | 0.0748 |
| | Height (mm) | 2.96 | 3.06 | 2.98 | 3.00 | 0.0432 |
| PCL@63sBG10 | Weight (g) | 0.27 | 0.24 | 0.22 | 0.24 | 0.0205 |
| | Diameter (mm) | 14.02 | 13.18 | 13.90 | 13.70 | 0.3709 |
| | Height (mm) | 3.04 | 2.96 | 3.02 | 3.01 | 0.0340 |
| | Weight (g) | 0.24 | 0.25 | 0.23 | 0.24 | 0.0082 |
| PCL@63sBG20 | Diameter (mm) | 12.04 | 12.96 | 13.02 | 12.67 | 0.4485 |
| | Height (mm) | 3.02 | 3.02 | 3.04 | 3.03 | 0.0094 |
| | Weight (g) | 0.29 | 0.22 | 0.27 | 0.26 | 0.0294 |

Our study provides a new method for the regeneration of non-load-bearing bone and small-volume bone defects. The consistent pore structure, which is essential for facilitating cellular in-growth, suggests that PCL/BG scaffolds, especially with the inclusion of bioactive glass, could potentially improve cellular integration and bone tissue regeneration. From Figure 4, we can observe that the scaffolds all have obvious pore structures formed by interleaved printed lines, which can provide space for cell growth. In addition, the consistency of these scaffolds with models ensures that they can be tailored for therapeutic applications, meeting the biological and mechanical requirements of bone regeneration.

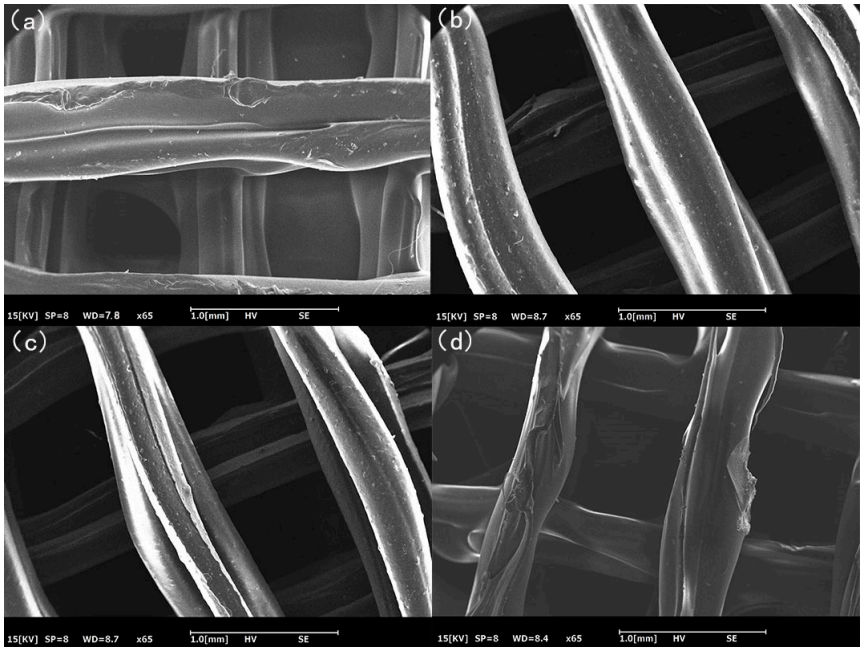


**Figure 4.** Micro morphology of composite scaffold (**a**) SEM image of pure PCL scaffold; (**b**) SEM image of the composite scaffold with a 5% 63s BG mass fraction; (**c**) SEM image of the composite scaffold with a 10% 63s BG mass fraction; (**d**) SEM image of the composite scaffold with a 20% 63s BG mass fraction.

From Figure 5, we can observe that PCL coated the powder after mixing with 63s BG powder.

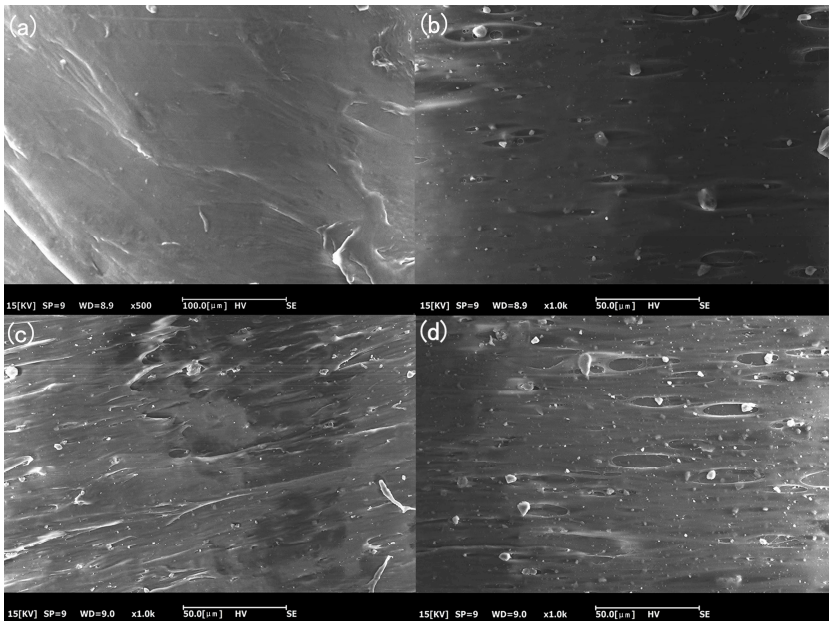


**Figure 5.** Micro morphology of composites: (**a**) SEM image of pure PCL; (**b**) SEM image of the composite with a 5% 63s BG mass fraction; (**c**) SEM image of the composite with a 10% 63s BG mass fraction; (**d**) SEM image of the composite with a 20% 63s BG mass fraction.

While our current study provides insights into the capabilities of PCL/BG scaffolds, there are several areas warranting further investigation:

Biocompatibility and cellular response: detailed in-vivo studies are needed to determine how cells respond to these scaffolds over extended periods, especially focusing on inflammation and foreign body reactions.

Degradation rates: understanding the degradation rates of PCL/BG scaffolds in various physiological conditions can help optimize their longevity and utility in bone regeneration applications.

Optimizing bioactive glass composition: different compositions of bioactive glass may offer varied benefits. It would be valuable to determine the optimal balance that maximizes regenerative potential while maintaining structural integrity.

Effect of printing parameters: given that melt flow rate can influence the success rate of printing, future studies could focus on refining the printing process to optimize scaffold characteristics.

### *3.2. X-ray Diffraction (XRD) Analysis*

As shown in Figure 6, since PCL is semi-crystalline and 63s BG is amorphous, we have observed that PCL has distinct characteristic peaks while 63s BG does not have sharp characteristic peaks. In their mixed materials, we can observe that the same characteristic peaks as PCL appear in different content groups, and no new characteristic peaks are generated, which indicates that no new crystals appear in the fimixed materials.

According to the principle of bioglass repair of bone defects, XRD and FTIR analysis and comparison of degradable composites can be carried out in future studies.

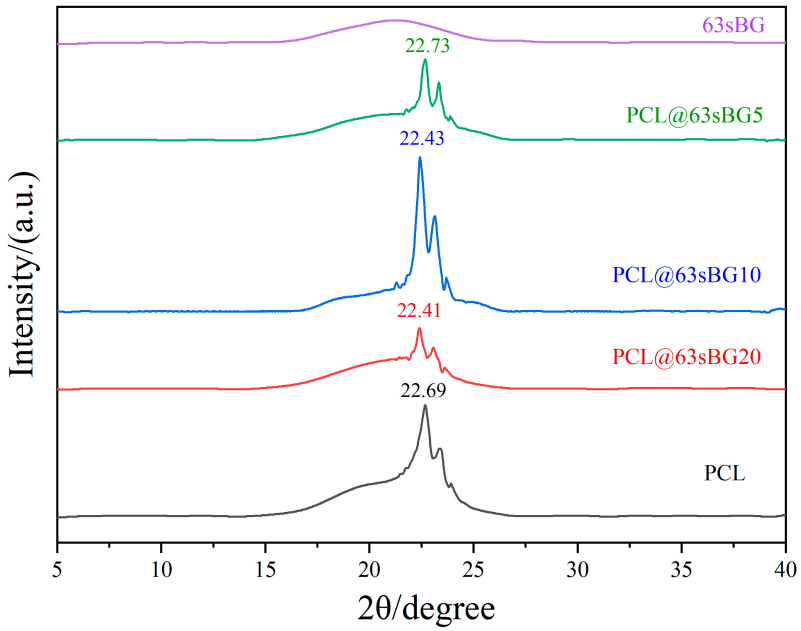


**Figure 6.** XRD pattern of the samples.

### *3.3. Melt Flow Rate of Composite Materials*

Our research, as depicted in Table 2, underscores the significant impact of integrating 63s BG into the composite material. The primary observation is that 63s BG serves as a filler, altering the composite's properties. One of the most pronounced changes is a reduction in the material's liquidity, leading to a distinct drop in its melt flow rate. This rate is pivotal in understanding the composite's ease of processing. The statistical method of single-factor analysis yielded a *p*-value of 0.00012, which is less than the predetermined significance level of 0.01. This indicates a substantial divergence between the groups under examination. More specifically, the results revealed a significant negative correlation between the augmented 63s BG content and the melt flow rate of the PCL-based composite bone scaffolds.

**Table 2.** Melt flow rate of composite materials (unit: g·10 $min^{-1}$; *p*-value < 0.01).

| Group \ Test Time | 1 | 2 | 3 | Average | σ |
|---|---|---|---|---|---|
| PCL | 5.94 | 6.48 | 6.54 | 6.32 | 0.33045 |
| PCL@63sBG5 | 5.40 | 5.22 | 6.06 | 5.56 | 0.44227 |
| PCL@63sBG10 | 4.62 | 4.44 | 5.10 | 4.72 | 0.34117 |
| PCL@63sBG20 | 3.96 | 4.02 | 4.02 | 4.00 | 0.03464 |

A reduced melt flow rate often signifies complications in various manufacturing techniques, such as injection molding or extrusion. Given this decline in processing property, there is a potential constraint on the material's suitability for specific industrial processes demanding high fluidity. Additionally, our findings indicate that the effect of 63s BG is not static; the melt flow rate decreases further as the 63s BG content rises. Thus, even minute changes in 63s BG concentration can significantly influence the material's processability.

Considering the substantial influence of 63s BG on the composite's characteristics, further research should focus on:

Optimizing 63s BG content: determining the ideal concentration of 63s BG that maximizes mechanical benefits while ensuring processability.

Alternative processing techniques: exploring other manufacturing processes that might be more compatible with the altered properties of the composite.

Material properties: investigating the long-term stability and mechanical strengths of composites with varying 63s BG concentrations.

### *3.4. Differential Scanning Calorimetry Result of Composite Materials*

From our detailed examination of the DSC curves in Figure 7, we deduced a correlation between the melting temperatures of 63s BG/PCL composites and the content of 63s BG. Notably, a progression from 52.33 °C in pure PCL to 53.18 °C with a 20% 63s BG composition was observed, emphasizing the role of 63s BG in modifying the thermal attributes of the PCL composite.

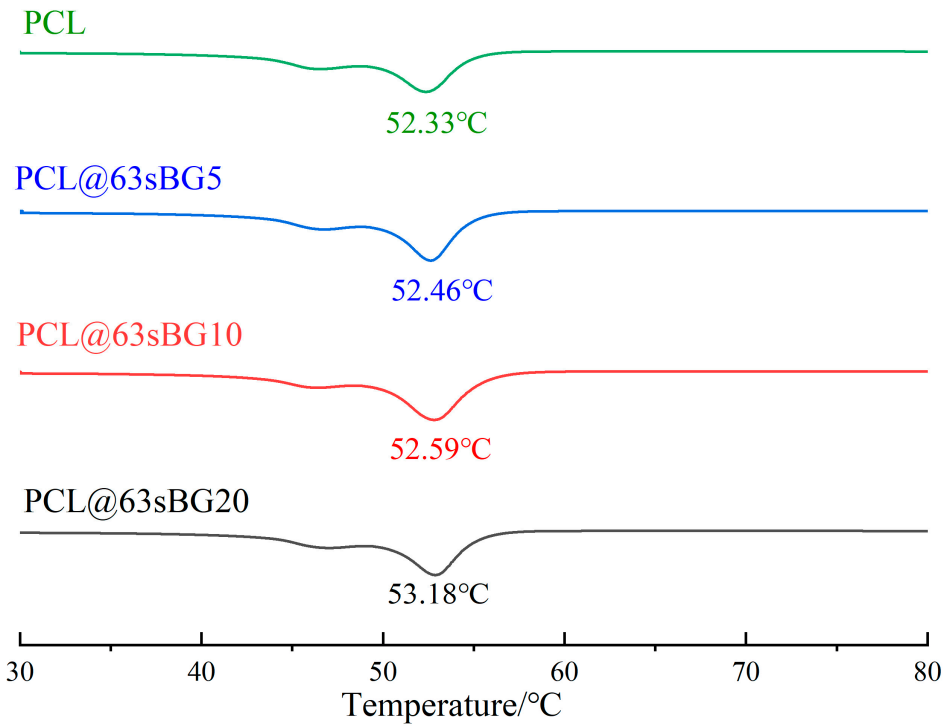


**Figure 7.** DSC curves of 63s BG/PCL composites with different 63s BG content.

The melting temperature of the composites increased with the addition of 63s BG. This phenomenon can likely be attributed to the interactions between the 63s BG and PCL, resulting in a more interconnected molecular arrangement.

Building on these insights, we suggest the following avenues for future exploration:

Interaction between 63s BG and PCL: a more in-depth analysis of how 63s BG interacts with PCL was conducted to investigate whether the addition of 63s BG will enhance the thermal stability of the composite.

Variability in BG content: exploring a wider range of 63s BG concentrations to see if there's an optimal concentration for balancing processability and thermal stability.

Long-term stability: conduct long-term tests to ascertain if the increased melting temperature directly impacts the longevity and performance of the composite in real-world applications.

Comparison with other bioactive glasses: investigating if other bioactive glass compositions produce similar effects on PCL or even amplify the observed thermal enhancements.

### *3.5. Contact Angles*

To investigate the effect of 63s BG addition on the hydrophilicity of PCL-based bone scaffolds, we conducted water contact angle tests on composite scaffolds with varying BG contents, as illustrated in Figure 8. Table 3 provides water contact angle measurements of both PCL and its composites with 63s BG. Across the board, we noted water contact angles below 90°, reflecting the hydrophilic nature of these materials. As the content

of 63s BG increases, the water contact angle delines from 88.23 ± 1.00° in pure PCL to 82.85 ± 0.97° with a 20% 63s BG composite. The statistical method of single-factor analysis yielded a *p*-value of 0.0197, which is less than the predetermined significance level of 0.05, indicating the presence of a substantial disparity between the groups. Specifically, it suggests a noteworthy positive association between the augmentation of 63s BG content and the water contact angle of the PCL-based composite bone scaffolds.

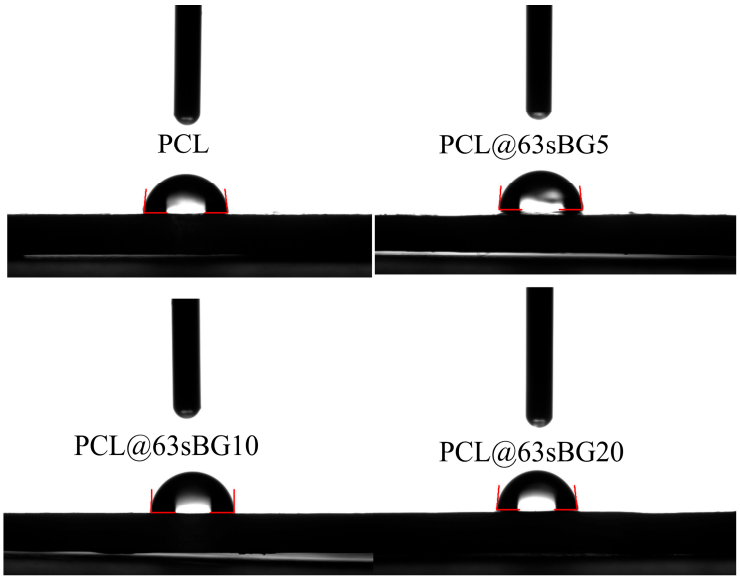


**Figure 8.** Hydrophilicity test images of each group of composites.

**Table 3.** Contact angle test results of composite scaffolds (unit: °; *p*-value < 0.05).

| Group \ Test Time | 1 | 2 | 3 | Average | σ |
|---|---|---|---|---|---|
| PCL | 87.36 | 88.01 | 89.33 | 88.23 | 1.00381 |
| PCL@63sBG5 | 84.11 | 85.95 | 89.26 | 86.44 | 2.60973 |
| PCL@63sBG10 | 85.41 | 86.76 | 88.07 | 86.75 | 1.33005 |
| PCL@63sBG20 | 81.73 | 83.33 | 83.49 | 82.85 | 0.97324 |

Such an inherent hydrophilic tendency is particularly auspicious for bone repair scaffolds. Hydrophilic surfaces are often preferred due to their propensity to promote cell adhesion, facilitate nutrient exchange, and ensure seamless tissue integration. The data indicates that 63s BG contributes more than just as a structural filler; it might enhance the scaffold's compatibility with biological environments. Even the observed nuanced reduction in contact angle is significant. In biological settings, marginal variations in surface properties can play pivotal roles in determining cell behavior and overall healing trajectories.

With these findings as a foundation, we advocate for the following research:

63s BG interaction mechanisms: delve into how 63s BG influences wettability at a molecular level, elucidating the exact mechanisms behind the increase in hydrophilicity.

Range of 63s BG concentrations: probe beyond the 20% concentration to discern if there is a saturation point or optimal concentration for hydrophilicity, balancing structural and biological benefits.

Biological response evaluation: conduct in-depth in vitro and in vivo studies to assess the cellular and tissue-level responses to scaffolds with varying 63s BG content.

Comparative studies: contrast PCL/63s BG scaffolds with other bioactive composite scaffolds to benchmark their performance and hydrophilic properties in bone repair contexts.

### *3.6. The Result of Rheology*

Figure 9 provides a comprehensive analysis of the rheological properties of the 63s BG/PCL composites, focusing on the storage modulus (G′), the loss modulus (G″), and the loss tangent (tan δ). These parameters are studied over a temperature range from 75 °C to 125 °C, offering insights into the material's thermal stability and behavior. Figure 9a reveals that the storage modulus, G′, decreases as the temperature increases, suggesting a decline in the material's stiffness with heat, a typical behavior for many polymeric materials [63,64]. However, this trend is counteracted by an increase in G′ with a greater 63s BG mass fraction, pointing to the reinforcing effect of 63s BG within the composite.

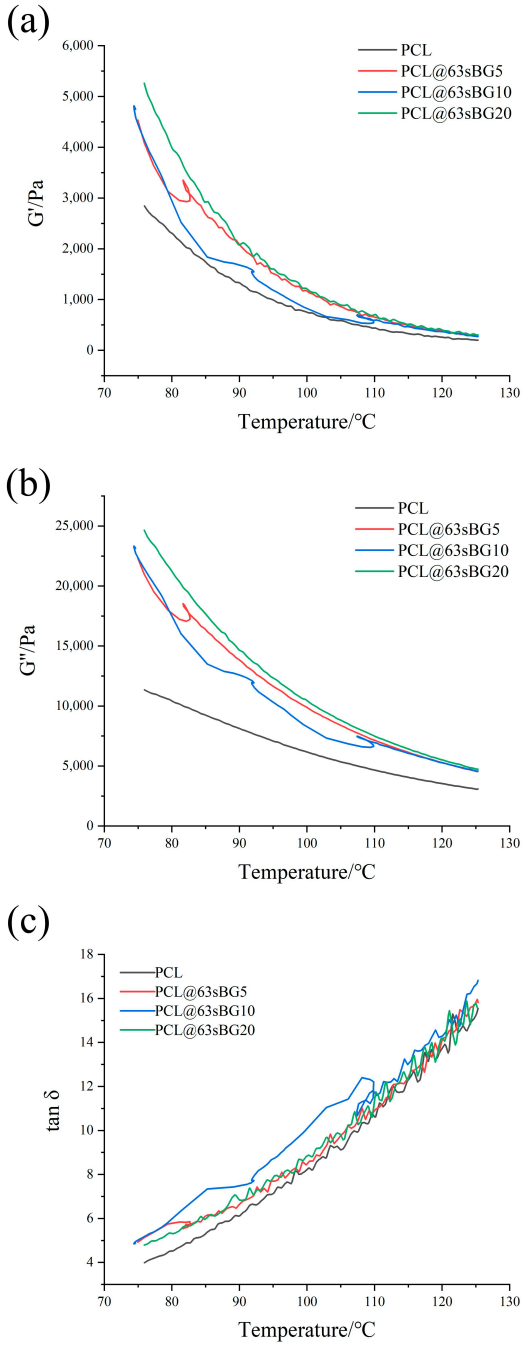


**Figure 9.** Slope rheology diagram of composites at 75–120 °C; (**a**) energy storage modulus (G′); (**b**) loss modulus (G″); (**c**) loss tangent (tan δ).

Figure 9b shows a similar trend for the loss modulus, G″, indicating that the material's ability to dissipate energy as heat also changes with temperature and 63s BG content [64]. The observed patterns could have significant implications for applications that require the composite to maintain specific mechanical properties over a range of temperatures. For example, in automotive or aerospace applications where thermal fluctuations are common, understanding these trends would be crucial. The intricate interplay between temperature and filler content in these composites suggests the need for a balanced optimization strategy to tailor the material properties for specific use cases.

### *3.7. Modulus of Elasticity*

Utilizing the GBT1041 test method, our research evaluated the elastic modulus of various composite samples, which include pure PCL and composites integrated with 5%, 10%, and 20% 63s BG content. The intent was to discern the effect of 63s BG on the mechanical attributes of the composite and its potential as a bone-mimicking material. However, inthe data accentuated that none of the composites achieved the rigorous mechanical specifications needed to simulate cortical bone, as shown in Figure 10.

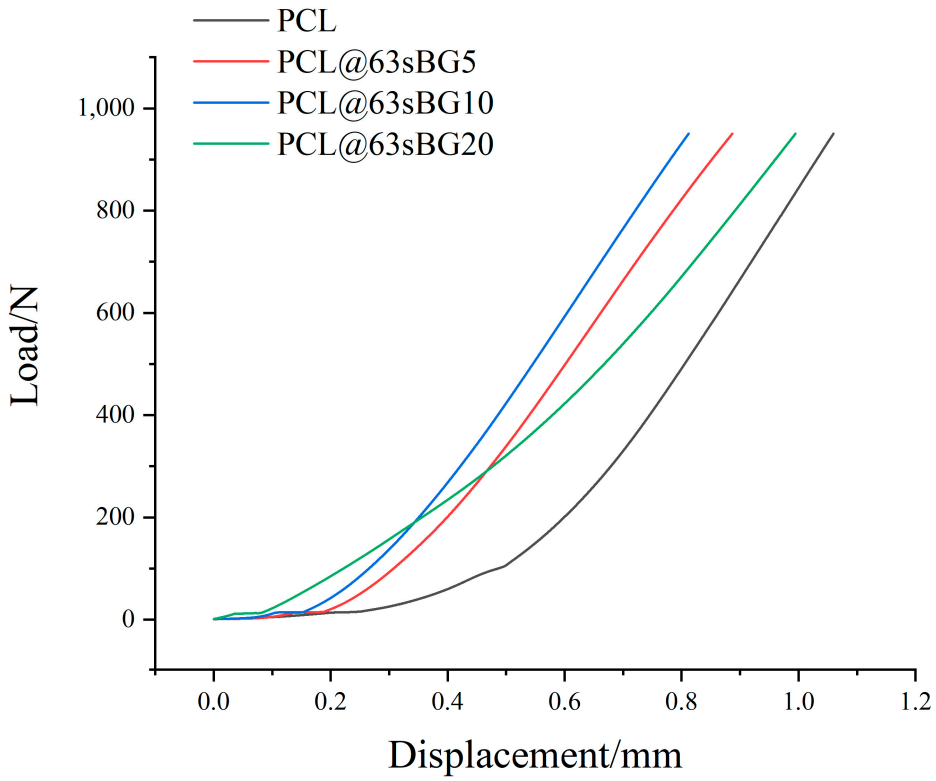


**Figure 10.** Elastic modulus of composite materials.

The elastic modulus of cortical bone is affected by many factors, such as age, sex, degree of mineralization, test direction (bone anisotropy), etc. Generally speaking, the elastic modulus of human cortical bone ranges from 10,000 N/mm$^2$ to 20,000 N/mm$^2$. The highest average modulus of elasticity in the sample is only 4.79977 N/mm$^2$ [65–70].

While the introduction of 63s BG does alter the elastic modulus, these modifications are not adequate to classify the composite as a suitable substitute for cortical bone. This presents a clear challenge in the quest for materials that can emulate bone properties, signaling a potential gap in current composite formulations.

Given the insights from our study, we propose the following avenues for extended investigation:

Alternative fillers: examining other potential fillers that could be synergized with PCL to meet the desired mechanical standards of cortical bone.

Fine-tuning component ratios: explore the proportions of 63s BG and other elements in the composite to determine the optimal mixture so that the composite can better promote bone repair.

Comparative analysis: comparing the performance of the 63s BG/PCL composite with other existing bone-mimicking materials to identify potential areas of improvement.

### *3.8. In Vitro Biodegradation of Composite Scaffolds*

To evaluate the biodegradation performance of the bone scaffold, weight loss rates were measured for a 50% porosity 63s BG/PCL composite bone scaffold and a 50% porosity PCL bone scaffold with varying 63s BG mass fractions in SBF over time.

Figure 11 delineates a clear positive correlation between the 63s BG mass fraction and the weight loss rate across specific time points. This directly indicates that the integration of 63s BG substantially augments the biodegradability of PCL scaffolds.

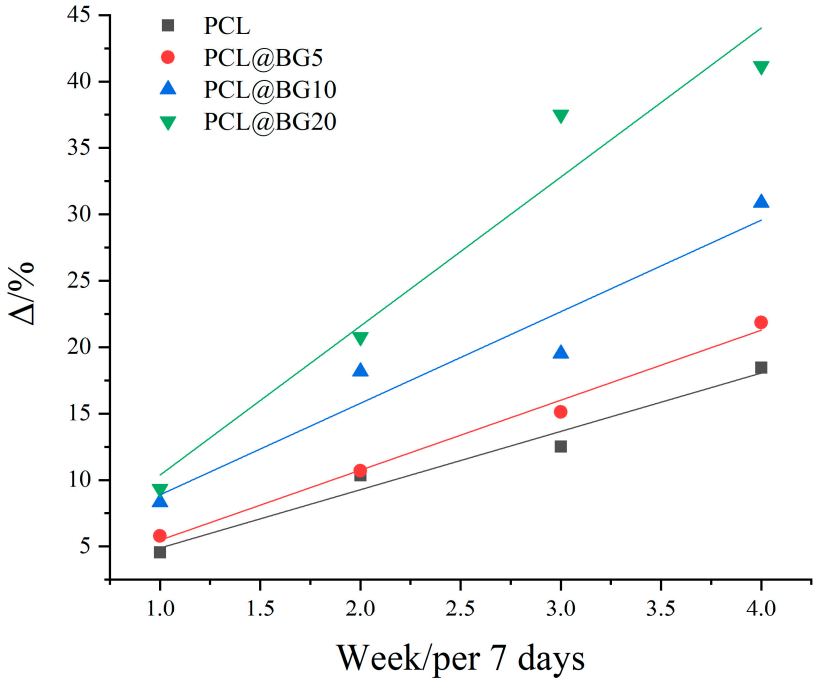


**Figure 11.** The weightlessness rate of each bracket at different time points.

Bone healing is an intricate physiological orchestration influenced by multifaceted factors such as bone type, defect specifics, individual age, health status, nutritional state, blood provisioning, and the stability of the defect or fracture. Given the findings, the swift initial degradation speed, paired with the accelerated degradation rate due to increased BG content, highlights a drawback. The composite scaffold, in its current form, might not be apt for managing critical bone defects, despite its enhanced biodegradability.

Drawing from the study's outcomes, we recommend delving into:

Optimizing BG content: exploring variations in BG concentrations to strike a balance between biodegradability and stability for bone repair.

Biodegradation mechanisms: investigating the molecular and structural changes during biodegradation to better understand and potentially manipulate the degradation rate.

Integration of other agents: research the incorporation of other biodegradable agents or components to modulate the scaffold's biodegradation rate.

Real-world applications: extensively testing the BG/PCL scaffold in real-world scenarios, including varied bone defect types and conditions, to ascertain its full range of applicability and limitations.

### *3.9. Alkaline Phosphatase Activity Detection*

MC3T3-E1 is a murine bone precursor cell line commonly used as a model for studying bone formation and mineralization. When they are cultured under specific conditions, these cells can produce mineralized nodules that mimic the process of bone mineralization. MC3T3-E1 cells are widely used to study bone formation, bone remodeling, and bone metabolism, as well as to evaluate the effects of bone biomaterials, drugs, and other therapies on bone cell function.

When alkaline phosphatase reacts with its substrate (BCIP), the substrate is dephosphorylated. This results in the formation of an intermediate product that can react with dyes such as phenolnitrate. The intermediate products produced by the reaction with the substrate bind to the dye, and they form a blue or purple precipitate at the site of alkaline phosphatase activity. This precipitate can be easily observed under a microscope, showing the exact location of the alkaline phosphatase. To ensure the accuracy of the results, the sample is fixed in advance.

From Figure 12, we can observe that after 3 days of normal culture, the cells were not stained, nor were the cells that were not in direct contact with the composite material, and the cells cultured in contact with the sample produced mineralized nodules and were stained. The results showed that the sample could promote osteogenic differentiation of cells. It is generally believed that BG can promote cell osteogenic differentiation, and the composite material containing 63s BG has better bone repair ability.

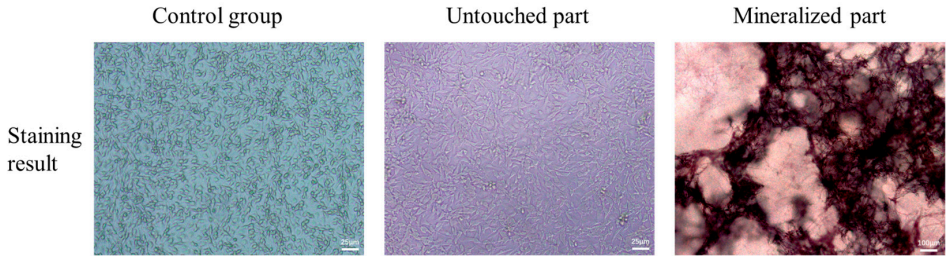


**Figure 12.** Staining after 72 h of cell culture.

Building on these findings, we propose:

Varied concentrations of 63s BG: investigating how different concentrations of 63s BG in the composite influence osteogenic differentiation to identify an optimal concentration.

Comparative analysis with other BGs: assessing how 63s BG performs in comparison to other types of bioactive glasses in promoting osteogenic differentiation and bone repair.

## 4. Conclusions

First, the inclusion of bioactive glass in the scaffold further enhances its regenerative potential, and bioactive glass is known for its ability to bind to living tissue, stimulate cell activity, and promote the deposition of extracellular matrix components. However, due to the low mechanical strength and fast initial degradation rate of the PCL/BG scaffold, it may not meet the requirements of weight-bearing bone implantation.

It can be observed from the results of the in vitro degradation rate that with the increase of BG content, the overall initial degradation rate of the scaffold further increases. The scaffold's degradation rate and ion release rate can be controlled by adjusting the content of 63s bioglass, which may help control the release of loaded drugs. It was observed from the sample compression results that the mechanical properties of PCL-based composites could not meet the mechanical strength of implanted load-bearing bone. However, it can be used to treat cartilage or non-weight-bearing bones. The hydrophilic surface of the composite makes it easier for cells to adhere and proliferate. In addition, rheological results show that the viscosity of the composite increases with the increase of 63s bioglass content, which may be due to the addition of powder, which increases the friction inside the material, or the reduction of free space in the fluid. This can be a hindrance in the 3D printing

process. From the results, we can observe that the composite material can promote cell mineralization. However, our limitation is that we have not been able to complete the testing of the thermal stability of the composite, the related properties after degradation, the specific effects on cells, and more in vivo experiments.

Moreover, the PCL/63s scaffold can be fabricated into various forms, such as porous structures or specific shapes, providing versatility in design and application. There are more applications for PCL/63s composites when combined with 3D printing. These different forms allow for tailored scaffolds with specific pore sizes, porosity, and surface characteristics, which can influence cell adhesion, migration, and differentiation. The high rate of degradation further opens up the possibility of using it to treat small-volume bone defects.

**Author Contributions:** Conceptualization, C.Z. and J.W.; methodology, S.C.; software, S.C. and Y.Q.; validation, Y.Z., G.F. and Z.L.; formal analysis, S.C.; investigation, Y.Q.; resources, C.Z., J.W. and G.F.; data curation, S.C. and Y.Q.; writing—original draft preparation, S.C. and Y.Q.; writing—review and editing, M.V. and C.Z.; visualization, Z.L.; supervision, J.W.; project administration, C.Z. and J.W.; funding acquisition, C.Z., J.W. and G.F. All authors have read and agreed to the published version of the manuscript.

**Funding:** This work was financially supported by Fujian Provincial Department of Science and technology joint innovation project (2023Y4021, 2020Y4018), the Research Project of Fashu Foundation of Fujian (MFK23014), Ningbo public welfare science and technology planning project (Grant No.: 2022S099), the regional development project of Fujian (Grant No.: 2022H4020, 2023H4023), and the Major Project of Science and Technology in Fuzhou (Grant No.: 2021-ZD-281), the Major Project of Science and Technology in FuJian (Grant No.: 2022NZ033021), and the Natural Science Foundation of Fujian Province, China (Grant No.: 2023N0038).

**Data Availability Statement:** Data are contained within the article.

**Conflicts of Interest:** The authors declare no conflict of interest.

## References

1. Henkel, J.; Woodruff, M.A.; Epari, D.R.; Steck, R.; Glatt, V.; Dickinson, I.C.; Choong, P.F.M.; Schuetz, M.A.; Hutmacher, D.W. Bone Regeneration Based on Tissue Engineering Conceptions—A 21st Century Perspective. *Bone Res.* **2013**, *1*, 216–248. [CrossRef]
2. Arealis, G.; Nikolaou, V.S. Bone printing: New frontiers in the treatment of bone defects. *Injury* **2015**, *46*, S20–S22. [CrossRef]
3. Calori, G.M.; Mazza, E.; Colombo, M.; Ripamonti, C. The use of bone-graft substitutes in large bone defects: Any specific needs? *Injury* **2011**, *42*, S56–S63. [CrossRef]
4. Bloemers, F.W.; Blokhuis, T.J.; Patka, P.; Bakker, F.C.; Wippermann, B.W.; Haarman, H.J.T.M. Autologous bone versus calcium-phosphate ceramics in treatment of experimental bone defects. *J. Biomed. Mater. Res. Part B Appl. Biomater.* **2003**, *66B*, 526–531. [CrossRef]
5. Gazdag, A.R.; Lane, J.M.; Glaser, D.; Forster, R.A. Alternatives to Autogenous Bone Graft: Efficacy and Indications. *JAAOS—J. Am. Acad. Orthop. Surg.* **1995**, *3*, 1–8. [CrossRef]
6. Ong, K.L.; Yun, B.M.; White, J.B. New biomaterials for orthopedic implants. *Orthop. Res. Rev.* **2015**, *7*, 107–130. [CrossRef]
7. Beaman, F.D.; Bancroft, L.W.; Peterson, J.J.; Kransdorf, M.J. Bone graft materials and synthetic substitutes. *Radiol. Clin.* **2006**, *44*, 451–461. [CrossRef]
8. Ian Gibson, I.G. *Additive Manufacturing Technologies 3D Printing, Rapid Prototyping, and Direct Digital Manufacturing*; Springer: Berlin/Heidelberg, Germany, 2015.
9. Guo, N.; Leu, M.C. Additive manufacturing: Technology, applications and research needs. *Front. Mech. Eng.* **2013**, *8*, 215–243. [CrossRef]
10. Mellor, S.; Hao, L.; Zhang, D. Additive manufacturing: A framework for implementation. *Int. J. Prod. Econ.* **2014**, *149*, 194–201. [CrossRef]
11. Gebler, M.; Schoot Uiterkamp, A.J.M.; Visser, C. A global sustainability perspective on 3D printing technologies. *Energy Policy* **2014**, *74*, 158–167. [CrossRef]
12. Kantaros, A.; Piromalis, D. Fabricating Lattice Structures via 3D Printing: The Case of Porous Bio-Engineered Scaffolds. *Appl. Mech.* **2021**, *2*, 289–302. [CrossRef]
13. Kantaros, A. Bio-Inspired Materials: Exhibited Characteristics and Integration Degree in Bio-Printing Operations. *Am. J. Eng. Appl. Sci.* **2022**, *15*, 255–263. [CrossRef]
14. Ventola, C.L. Medical Applications for 3D Printing: Current and Projected Uses. *Pharm. Ther.* **2014**, *39*, 704–711.

15. Kostakis, V.; Niaros, V.; Giotitsas, C. Production and governance in hackerspaces: A manifestation of Commons-based peer production in the physical realm? *Int. J. Cult. Stud.* **2014**, *18*, 555–573. [CrossRef]
16. Murphy, S.V.; Atala, A. 3D bioprinting of tissues and organs. *Nat. Biotechnol.* **2014**, *32*, 773–785. [CrossRef]
17. Trenfield, S.J.; Awad, A.; Goyanes, A.; Gaisford, S.; Basit, A.W. 3D Printing Pharmaceuticals: Drug Development to Frontline Care. *Trends Pharmacol. Sci.* **2018**, *39*, 440–451. [CrossRef] [PubMed]
18. Gibson, I.; Rosen, D.W.; Stucker, B.; Khorasani, M.; Rosen, D.; Stucker, B.; Khorasani, M. *Additive Manufacturing Technologies*; Springer: Berlin/Heidelberg, Germany, 2021; Volume 17.
19. Gross, B.C.; Erkal, J.L.; Lockwood, S.Y.; Chen, C.; Spence, D.M. Evaluation of 3D Printing and Its Potential Impact on Biotechnology and the Chemical Sciences. *Anal. Chem.* **2014**, *86*, 3240–3253. [CrossRef] [PubMed]
20. Ma, P.X.; Zhang, R. Synthetic nano-scale fibrous extracellular matrix. *J. Biomed. Mater. Res. Off. J. Soc. Biomater. Jpn. Soc. Biomater. Aust. Soc. Biomater.* **1999**, *46*, 60–72. [CrossRef]
21. Xu, C.; Inai, R.; Kotaki, M.; Ramakrishna, S. Electrospun nanofiber fabrication as synthetic extracellular matrix and its potential for vascular tissue engineering. *Tissue Eng.* **2004**, *10*, 1160–1168. [CrossRef] [PubMed]
22. Bose, S.; Vahabzadeh, S.; Bandyopadhyay, A. Bone tissue engineering using 3D printing. *Mater. Today* **2013**, *16*, 496–504. [CrossRef]
23. Rezwan, K.; Chen, Q.Z.; Blaker, J.J.; Boccaccini, A.R. Biodegradable and bioactive porous polymer/inorganic composite scaffolds for bone tissue engineering. *Biomaterials* **2006**, *27*, 3413–3431. [CrossRef] [PubMed]
24. Venkatesan, J.; Kim, S.-K.; Shim, M.S. Antimicrobial, antioxidant, and anticancer activities of biosynthesized silver nanoparticles using marine algae Ecklonia cava. *Nanomaterials* **2016**, *6*, 235. [CrossRef] [PubMed]
25. Thurzo, A.; Gálfiová, P.; Nováková, Z.V.; Polák, Š.; Varga, I.; Strunga, M.; Urban, R.; Surovková, J.; Leško, L.; Hajdúchová, Z.; et al. Fabrication and In Vitro Characterization of Novel Hydroxyapatite Scaffolds 3D Printed Using Polyvinyl Alcohol as a Thermoplastic Binder. *Int. J. Mol. Sci.* **2022**, *23*, 14870. [CrossRef]
26. Mironov, V.; Visconti, R.P.; Kasyanov, V.; Forgacs, G.; Drake, C.J.; Markwald, R.R. Organ printing: Tissue spheroids as building blocks. *Biomaterials* **2009**, *30*, 2164–2174. [CrossRef] [PubMed]
27. Kantaros, A. 3D Printing in Regenerative Medicine: Technologies and Resources Utilized. *Int. J. Mol. Sci.* **2022**, *23*, 14621. [CrossRef]
28. Ozbolat, I.T.; Hospodiuk, M. Current advances and future perspectives in extrusion-based bioprinting. *Biomaterials* **2016**, *76*, 321–343. [CrossRef]
29. Groll, J.; Boland, T.; Blunk, T.; Burdick, J.A.; Cho, D.-W.; Dalton, P.D.; Derby, B.; Forgacs, G.; Li, Q.; Mironov, V.A.; et al. Biofabrication: Reappraising the definition of an evolving field. *Biofabrication* **2016**, *8*, 013001. [CrossRef] [PubMed]
30. Jakus, A.E.; Rutz, A.L.; Jordan, S.W.; Kannan, A.; Mitchell, S.M.; Yun, C.; Koube, K.D.; Yoo, S.C.; Whiteley, H.E.; Richter, C.-P.; et al. Hyperelastic "bone": A highly versatile, growth factor–free, osteoregenerative, scalable, and surgically friendly biomaterial. *Sci. Transl. Med.* **2016**, *8*, 358ra127. [CrossRef]
31. Woodruff, M.A.; Hutmacher, D.W. The return of a forgotten polymer—Polycaprolactone in the 21st century. *Prog. Polym. Sci.* **2010**, *35*, 1217–1256. [CrossRef]
32. Sun, H.; Mei, L.; Song, C.; Cui, X.; Wang, P. The in vivo degradation, absorption, and excretion of PCL-based implant. *Biomaterials* **2006**, *27*, 1735–1740. [CrossRef]
33. Labet, M.; Thielemans, W. Synthesis of polycaprolactone: A review. *Chem. Soc. Rev.* **2009**, *38*, 3484–3504. [CrossRef] [PubMed]
34. Serrano, M.C.; Chung, E.J.; Ameer, G.A. Advances and applications of biodegradable elastomers in regenerative medicine. *Adv. Funct. Mater.* **2010**, *20*, 192–208. [CrossRef]
35. Damle, M.; Mallya, R. Development and evaluation of a novel delivery system containing phytophospholipid complex for skin aging. *AAPS PharmSciTech* **2016**, *17*, 607–617. [CrossRef] [PubMed]
36. Temple, J.P.; Hutton, D.L.; Hung, B.P.; Huri, P.Y.; Cook, C.A.; Kondragunta, R.; Jia, X.; Grayson, W.L. Engineering anatomically shaped vascularized bone grafts with hASCs and 3D-printed PCL scaffolds. *J. Biomed. Mater. Res. Part A* **2014**, *102*, 4317–4325. [CrossRef]
37. Nair, L.S.; Laurencin, C.T. Biodegradable polymers as biomaterials. *Prog. Polym. Sci.* **2007**, *32*, 762–798. [CrossRef]
38. Ghorbani, F.M.; Kaffashi, B.; Shokrollahi, P.; Seyedjafari, E.; Ardeshirylajimi, A. PCL/chitosan/Zn-doped nHA electrospun nanocomposite scaffold promotes adipose-derived stem cells adhesion and proliferation. *Carbohydr. Polym.* **2015**, *118*, 133–142. [CrossRef]
39. Ji, W.; Sun, Y.; Yang, F.; van den Beucken, J.J.J.P.; Fan, M.; Chen, Z.; Jansen, J.A. Bioactive Electrospun Scaffolds Delivering Growth Factors and Genes for Tissue Engineering Applications. *Pharm. Res.* **2011**, *28*, 1259–1272. [CrossRef] [PubMed]
40. Sinha, V.R.; Bansal, K.; Kaushik, R.; Kumria, R.; Trehan, A. Poly-ϵ-caprolactone microspheres and nanospheres: An overview. *Int. J. Pharm.* **2004**, *278*, 1–23. [CrossRef]
41. Ma, Z.; Gao, C.; Gong, Y.; Shen, J. Paraffin spheres as porogen to fabricate poly(L-lactic acid) scaffolds with improved cyto-compatibility for cartilage tissue engineering. *J. Biomed. Mater. Res. Part B Appl. Biomater.* **2003**, *67B*, 610–617. [CrossRef] [PubMed]
42. Hench, L.L. The story of Bioglass®. *J. Mater. Sci. Mater. Med.* **2006**, *17*, 967–978. [CrossRef]
43. Rahaman, M.N.; Day, D.E.; Sonny Bal, B.; Fu, Q.; Jung, S.B.; Bonewald, L.F.; Tomsia, A.P. Bioactive glass in tissue engineering. *Acta Biomater.* **2011**, *7*, 2355–2373. [CrossRef]
44. Hench, L.L. Bioactive materials: The potential for tissue regeneration. *J. Biomed. Mater. Res.* **1998**, *41*, 511–518. [CrossRef]

45. Hench, L.L.; Polak, J.M. Third-Generation Biomedical Materials. *Science* **2002**, *295*, 1014–1017. [CrossRef] [PubMed]
46. Jones, J.R. Review of bioactive glass: From Hench to hybrids. *Acta Biomater.* **2013**, *9*, 4457–4486. [CrossRef]
47. Hoppe, A.; Güldal, N.S.; Boccaccini, A.R. A review of the biological response to ionic dissolution products from bioactive glasses and glass-ceramics. *Biomaterials* **2011**, *32*, 2757–2774. [CrossRef] [PubMed]
48. Baino, F.; Vitale-Brovarone, C. Three-dimensional glass-derived scaffolds for bone tissue engineering: Current trends and forecasts for the future. *J. Biomed. Mater. Res. Part A* **2011**, *97A*, 514–535. [CrossRef]
49. Zhang, D.; Leppäranta, O.; Munukka, E.; Ylänen, H.; Viljanen, M.K.; Eerola, E.; Hupa, M.; Hupa, L. Antibacterial effects and dissolution behavior of six bioactive glasses. *J. Biomed. Mater. Res. Part A* **2010**, *93A*, 475–483. [CrossRef]
50. Miguez-Pacheco, V.; Hench, L.L.; Boccaccini, A.R. Bioactive glasses beyond bone and teeth: Emerging applications in contact with soft tissues. *Acta Biomater.* **2015**, *13*, 1–15. [CrossRef] [PubMed]
51. Bari, A.; Bloise, N.; Fiorilli, S.; Novajra, G.; Vallet-Regí, M.; Bruni, G.; Torres-Pardo, A.; González-Calbet, J.M.; Visai, L.; Vitale-Brovarone, C. Copper-containing mesoporous bioactive glass nanoparticles as multifunctional agent for bone regeneration. *Acta Biomater.* **2017**, *55*, 493–504. [CrossRef]
52. Islam, M.T.; Felfel, R.M.; Abou Neel, E.A.; Grant, D.M.; Ahmed, I.; Hossain, K.M.Z. Bioactive calcium phosphate–based glasses and ceramics and their biomedical applications: A review. *J. Tissue Eng.* **2017**, *8*, 2041731417719170. [CrossRef]
53. Chen, J.; Xing, Y.; Bai, X.; Xue, M.; Shi, Q.; Li, B. Strong Bioactive Glass-Based Hybrid Implants with Good Biomineralization Activity Used to Reduce Formation Duration and Improve Biomechanics of Bone Regeneration. *Polymers* **2023**, *15*, 3497. [CrossRef] [PubMed]
54. Daraei, J. Production and characterization of PCL (Polycaprolactone) coated TCP/nanoBG composite scaffolds by sponge foam method for orthopedic applications. *J. Compos. Compd.* **2020**, *2*, 44–49. [CrossRef]
55. Li, W.; Nooeaid, P.; Roether, J.A.; Schubert, D.W.; Boccaccini, A.R. Preparation and characterization of vancomycin releasing PHBV coated 45S5 Bioglass®-based glass–ceramic scaffolds for bone tissue engineering. *J. Eur. Ceram. Soc.* **2014**, *34*, 505–514. [CrossRef]
56. Eqtesadi, S.; Motealleh, A.; Pajares, A.; Guiberteau, F.; Miranda, P. Influence of sintering temperature on the mechanical properties of ϵ-PCL-impregnated 45S5 bioglass-derived scaffolds fabricated by robocasting. *J. Eur. Ceram. Soc.* **2015**, *35*, 3985–3993. [CrossRef]
57. Jones, J.R. Reprint of Review of bioactive glass: From Hench to hybrids. *Acta Biomater.* **2015**, *23*, S53–S82. [CrossRef]
58. O'Donnell, M.D.; Watts, S.J.; Hill, R.G.; Law, R.V. The effect of phosphate content on the bioactivity of soda-lime-phosphosilicate glasses. *J. Mater. Sci. Mater. Med.* **2009**, *20*, 1611–1618. [CrossRef]
59. Baino, F.; Hamzehlou, S.; Kargozar, S. Bioactive Glasses: Where Are We and Where Are We Going? *J. Funct. Biomater.* **2018**, *9*, 25. [CrossRef]
60. Wang, Z.; Yao, R.; Wang, D.; Wang, H.; Liang, C. Structure design and biological evaluation of the mechanical-adaptive titanium-based porous implants. *Mater. Technol.* **2021**, *36*, 851–856. [CrossRef]
61. Gregor, A.; Filová, E.; Novák, M.; Kronek, J.; Chlup, H.; Buzgo, M.; Blahnová, V.; Lukášová, V.; Bartoš, M.; Nečas, A. Designing of PLA scaffolds for bone tissue replacement fabricated by ordinary commercial 3D printer. *J. Biol. Eng.* **2017**, *11*, 31. [CrossRef]
62. Isaacson, N.; Lopez-Ambrosio, K.; Chubb, L.; Waanders, N.; Hoffmann, E.; Witt, C.; James, S.; Prawel, D.A. Compressive properties and failure behavior of photo cast hydroxyapatite gyroid scaffolds vary with porosity. *J. Biomater. Appl.* **2022**, *37*, 55–76. [CrossRef]
63. Estevam Barbosa de Las, C.; João Batista, N., Jr.; Elissa, T.; Willian Henrique, V.; Tulimar, P.M.C.; Iracema Maria Utsch, B.; Carlos Alberto, C., Jr.; Rodrigo Guerra, P. Residual Stresses and Cracking in Dental Restorations due to Resin Contraction Considering In-Depth Young's Modulus Variation. In *Applied Biological Engineering*; Ganesh, R.N., Ed.; IntechOpen: Rijeka, Croatia, 2012; p. Ch. 25.
64. Vaddi, J.S.; Holland, S.D.; Kessler, M.R. Loss modulus measurement of a viscoelastic polymer at acoustic and ultrasonic frequencies using vibrothermography. *Measurement* **2021**, *168*, 108311. [CrossRef]
65. Rho, J.-Y.; Kuhn-Spearing, L.; Zioupos, P. Mechanical properties and the hierarchical structure of bone. *Med. Eng. Phys.* **1998**, *20*, 92–102. [CrossRef] [PubMed]
66. Currey, J.D. The effect of porosity and mineral content on the Young's modulus of elasticity of compact bone. *J. Biomech.* **1988**, *21*, 131–139. [CrossRef] [PubMed]
67. Morgan, E.F.; Keaveny, T.M. Dependence of yield strain of human trabecular bone on anatomic site. *J. Biomech.* **2001**, *34*, 569–577. [CrossRef] [PubMed]
68. Fung, Y.-C. *Biomechanics: Mechanical Properties of Living Tissues*; Springer Science & Business Media: Berlin/Heidelberg, Germany, 2013.
69. Turner, C.H.; Burr, D.B. Basic biomechanical measurements of bone: A tutorial. *Bone* **1993**, *14*, 595–608. [CrossRef]
70. Zysset, P.K.; Guo, X.E.; Hoffler, C.E.; Moore, K.E.; Goldstein, S.A. Elastic modulus and hardness of cortical and trabecular bone lamellae measured by nanoindentation in the human femur. *J. Biomech.* **1999**, *32*, 1005–1012. [CrossRef] [PubMed]